CHEMISTRY
A EUROPEAN JOURNAL

DOI: 10.1002/chem.200500416

Triple Hydrogen Bonds Direct Crystal Engineering of Metal-Assembled Complexes: The Effect of a Novel Organic–Inorganic Module on Supramolecular Structure

Keiichi Adachi,[a] Yuichi Sugiyama,[b] Ko Yoneda,[a] Koichi Yamada,[a] Koichi Nozaki,[a] Akira Fuyuhiro,[a] and Satoshi Kawata*[a]

Abstract: Novel triply hydrogen bonded suprastructures based on $[M(tdpd)_2(L)_2]^{2-}$ (H_2tdpd = 1,4,5,6-tetrahydro-5,6-dioxo-2,3-pyrazinedicarbonitrile, L = solvent) and melamine-analogous cations have been synthesized and characterized. The use of anions containing two AAA sets from $[M(tdpd)_2(L)_2]^{2-}$ together with cations containing one DDD set (A = hydrogen-bond acceptor, D = hydrogen-bond donor) leads to the formation of complementary triply hydrogen bonded modules in the solid state. In all cases, the building module is further extended via additional hydrogen-bonding interactions to produce a tape, and tapes are assembled into sheets. These results show that a hydrogen-bonded module consisting of different kinds of building blocks, one of which is a metal complex that includes hydrogen-bond acceptor sites and the other is a hydrogen-bond donor molecule, will be attractive for constructing metal-containing supramolecular systems by the self-assembly technique.

Keywords: crystal engineering · hydrogen bonds · layered compounds · self-assembly · supramolecular chemistry

Introduction

The hydrogen-bonding interaction, which plays a fundamental role in the structure of DNA and in the secondary and tertiary structure of proteins, is also responsible for some of the anomalous properties of many important compounds, for example, water, ammonia, and hydrogen fluoride.[1] Hydrogen bonding also exerts important effects on the organization and properties of many solid-state materials.[2] The selectivity and directivity of the hydrogen bond have also been instrumental in the preparation of a variety of distinctive and predictable structural aggregates, notably in molecular solids, and the use of hydrogen bonding as a steering force is now beginning to emerge as the most important strategy in crystal engineering.[3] On the other hand, noncovalent interactions play a critical role in mediating a range of thermal and photoinduced biological electron-transfer processes.[4,5] Although subject to considerable theoretical[6] and experimental[7] scrutiny, the fundamental principles of how such interactions mediate electron-transfer reactions remain recondite. For this reason, simple model systems that would allow the underlying chemical and photochemical events to be probed with greater precision have been developed. In this context, particular attention has focused on self-assembled ensembles formed by hydrogen bonds.[5,8]

The incorporation of metals into supramolecular systems has recently attracted some attention because it generates the possibility of introducing the well-developed redox, optical, adsorption, and magnetic properties of transition metals into these systems.[9,10] Our approach and that of others in this area has been to prepare complexes of ligands which have both metal-coordination and hydrogen-bonding sites.[10–12] By judicious choice of complementary hydrogen-bonding components, dimers, tapes, sheets, and so on have been generated in the solid state.[13] The presence of metal ions in these systems introduces many additional potential variables that continue to be explored.

The $tdpd^{2-}$ (H_2tdpd = 1,4,5,6-tetrahydro-5,6-dioxo-2,3-pyrazinedicarbonitrile) anion attracted our interest as a potential bifunctional ligand with hydrogen-bonding characteris-

[a] Dr. K. Adachi, K. Yoneda, Dr. K. Yamada, Dr. K. Nozaki, Dr. A. Fuyuhiro, Prof. S. Kawata
Department of Chemistry, Graduate School of Science
Osaka University, Toyonaka, Osaka 560-0043 (Japan)
Fax: (+81) 6-6850-5473
E-mail: kawata@chem.sci.osaka-u.ac.jp

[b] Y. Sugiyama
Department of Chemistry, Shizuoka University
Ohya, Shizuoka, 422-8529 (Japan)

Supporting information for this article is available on the WWW under http://www.chemeurj.org/ or from the author.

tics.[14,15] This dianion has both multiple metal-binding and multiple hydrogen bonding sites. Recently, we established that the use of anions containing two AAA sets from $[M(tdpd)_2(H_2O)_2]^{2-}$ together with melaminium cations[16] containing one DDD set (A = hydrogen bond acceptor, D = hydrogen bond donor) leads to the formation of complementary triply hydrogen bonded modules in the solid state, even when the products are crystallized from a competitive solvent such as water (Scheme 1).[15] In all cases, the building

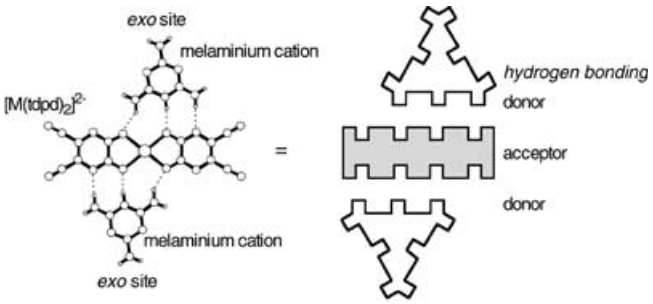

Scheme 1.

module is further extended by additional hydrogen-bonding interactions to produce tapes, and tapes are assembled into sheets (Scheme 2). These results show that a hydrogen-bonded module consisting of different kinds of building blocks, one of which is a metal complex that includes hydrogen-bond acceptor sites and the other is a hydrogen-bond donor molecule, will be interesting for constructing metal-containing supramolecular system by the self-assembly technique.

Theoretical calculations and experimental data have indicated that triple hydrogen-bonding interactions between two molecules in which all A sites are localized on one component and all D sites on the other (i.e., AAA/DDD) are stronger than those in which the A and D sites are distributed between the two molecules (i.e., ADA/DAD, AAD/DDA).[17] Therefore, it is interesting and challenging to construct suprastructures based on crystal engineering with charge-augmented AAA/DDD triple hydrogen bonds and intermolecular interactions within the modules. If the exogenous site (*exo* site in Scheme 1) of the module $[Hmel]_2[M(tdpd)_2(H_2O)_2]$ can be replaced by a different kind of functional group, the resulting structure can be controlled by using the new module as a topological director of crystal packing:[12] When a functional group that has no hydrogen-bonding site is introduced into the *exo* site, the above-mentioned two-dimensional sheet structures may assemble into different structures. Furthermore, the functional moiety of the *exo* site controls the hydrogen-bonding properties but does not affect the potential to form the cation–anion–cation module. In this study we synthesized novel triply hydrogen bonded modules based suprastructures of $[M(tdpd)_2(L)_2]$ with melamine analogues (Scheme 3) by crystal engineering. The crystallographic and physicochemical characterization of these compounds are also described. The crystal structures of these compounds consist of similar kinds of modules that are made of a simple synthon.

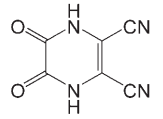

H_2tdpd

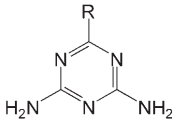

R	
$-NH_2$:	mel
–phenyl :	bg
$-N(CH_2CH{=}CH_2)_2$:	damel
–heptyl :	dhtz
–(9-phenanthryl) :	dptz

Scheme 3.

Results and Discussion

Crystal structures of $[Hbg]_2[M^{II}(tdpd)_2(MeOH)_2]\cdot 4MeOH$ (M^{II} = Ni (1), Co (2), bg = benzoguanamine) and $[Hbg]_2[Cu^{II}(tdpd)_2]\cdot 2MeOH$ (3): X-ray crystallography revealed that **1** and **2** are isostructural. The structure of **1** consists of mononuclear $[Ni(tdpd)_2(MeOH)_2]^{2-}$ dianions, Hbg^+ cations, and interstitial methanol molecules. An ORTEP plot of **1** is shown in Figure 1a. The atom numbering scheme of **2** is the same as that of **1**. The coordination geometry around the nickel ion is a distorted octahedron involving the four oxygen atoms

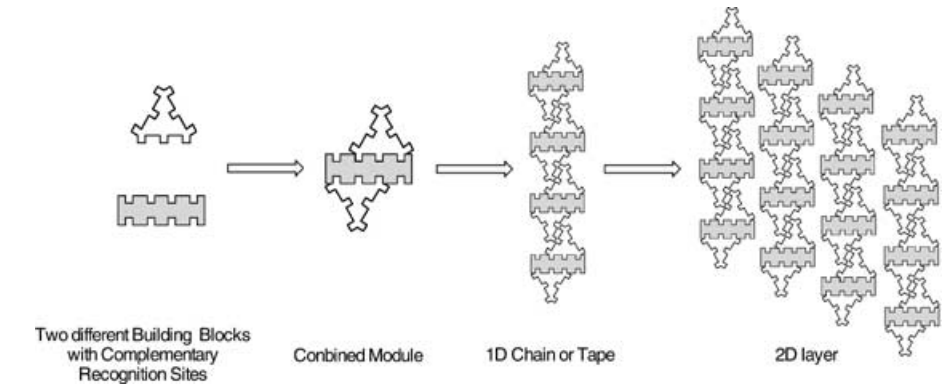

Scheme 2.

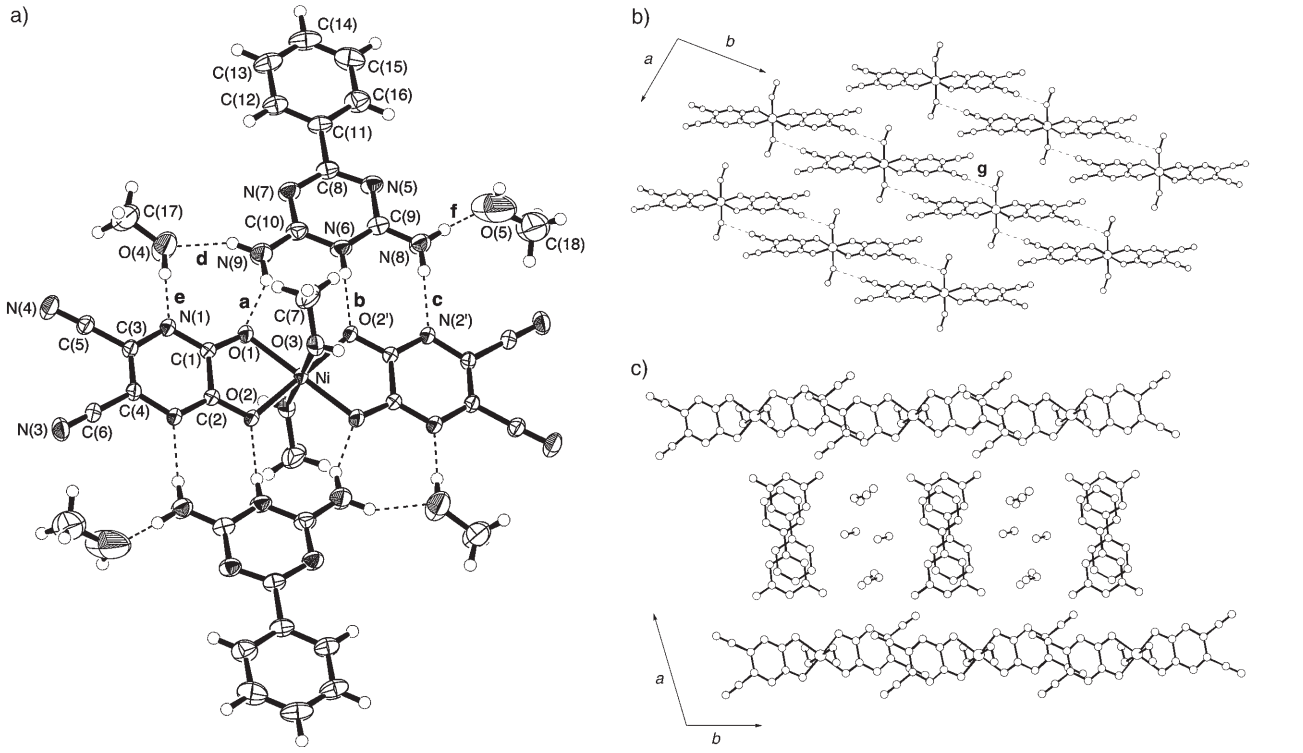

Figure 1. a) ORTEP plot of **1** with labeling scheme and thermal ellipsoids at the 50% probability level for Ni, O, N, and C atoms. Spheres of the hydrogen atoms have been arbitrarily reduced. Hydrogen-bonding parameters: N···N/O, H···N/O distances [Å], N/O–H···N/O angles [°]: **a** 2.839(3), 2.03, 172; **b** 2.817(2), 1.99, 176; **c** 2.914(3), 2.04, 173; **d** 2.799(4), 2.01, 144; **e** 2.862(3), 1.93, 177, **f** 2.801(4), 1.94, 165. b) Part of the hydrogen-bonded planar layers formed by **1** showing the intermolecular interactions between adjacent complexes. Hydrogen-bonding parameters: N···O, H···N distances [Å], O–H···N angles [°]: **g** 2.842(2), 2.18, 169. Hydrogen atoms are omitted for clarity. c) View of the assembled structure of **1** showing that the hydrogen-bonded layers are interlinked by π–π stacking to form channels. The channels are filled with methanol molecules.

of two $tdpd^{2-}$ anions and the two oxygen atoms from two methanol molecules (Ni–O(1), Ni–O(1′) 2.001(1); Ni–O(2), Ni–O(2′) 2.046(1); Ni–O(3), Ni–O(3′) 2.109(1) Å). The $[Ni(tdpd)_2(MeOH)_2]^{2-}$ dianions are linked to the Hbg^+ ions through an AAA/DDD triple hydrogen bond (O(1)···N(9) 2.839(4), O(2′)···N(6) 2.817(4), N(2′)···N(8) 2.914(4) Å; **a**, **b** and **c**, respectively, in Figure 1a). The triply hydrogen bonded network of the anionic complex with the Hbg^+ cations forms the building module. The module of compound **1** is similar to that of the series $[Hmel]_2[M(tdpd)_2(L)_m]$ in Scheme 1,[15] but the assembled structure of **1** is different due to the introduction of the phenyl group on the *exo* site of the module: the $[Hbg]_2[Ni(tdpd)_2(MeOH)_2]$ modules in **1** form a layer with completely different structural features from those of $[Hmel]_2[M(tdpd)_2(H_2O)_2]$. The layer is supported by hydrogen bonds[10,22] between the coordinated methanol molecules and the nitrogen atoms of nitrile groups on the $tdpd^{2-}$ anions (**g** in Figure 1b) and stacking interactions between the nitrile groups of the $tdpd^{2-}$ ions on adjacent complexes (spacing 3.27–3.53 Å). The phenyl moieties of the Hbg^+ cation protrude into the interlayer region. Adjacent layers are connected by π–π stacking interactions between the triazine rings and the phenyl groups of the Hbg^+ cation from adjacent layers (spacing 3.46–3.63 Å), resulting in a three-dimensional network with channels (Figure 1c). The interlayer distance, defined as the perpendicular distance between the layers, is 13.71 Å. The two methanol molecules in the channels form hydrogen bonds to the nitrogen atoms of the pyrazine rings or the side-chain nitrogen atoms of the Hbg^+ cation (**d**, **e**, and **f** in Figure 1a).

The structure of $[Hbg]_2[Cu^{II}(tdpd)_2]\cdot 2MeOH$ (**3**) consists of mononuclear $[Cu(tdpd)_2]^{2-}$ dianions, Hbg^+ cations, and uncoordinated methanol molecules. An ORTEP plot of the structure around the copper ion in **3** with the atom numbering scheme is shown in Figure 2a. The structure of **3** shows that the desired coordination and aggregation have been achieved: the copper atom is coordinated to the two $tdpd^{2-}$ anions, which are in turn involved in AAA/DDD-type hydrogen bonding with the Hbg^+ cations. The coordination geometry around the copper ion in the monomer involves the four oxygen atoms of the $tdpd^{2-}$ ion and is square-planar (Cu–O(1), Cu–O(1′) 1.900(2); Cu–O(2), Cu–O(2′) 1.947(2) Å). The three hydrogen bonding distances between the $tdpd^{2-}$ ion and the Hbg^+ cation units are O(1)···N(9′) 2.838(3), O(2′)···N(6), 2.820(3), and N(2′)···N(8) 2.942(4) Å (**a**, **b** and **c**, respectively, in Figure 2a). The triply hydrogen bonded network of the anionic complex with the Hbg^+ cations forms the building module. The $[Hbg]_2[Cu(tdpd)_2]$ module is linked to the adjacent modules by additional N(H)···N hydrogen bonds (**e** in Figure 2b) to form one-dimensional chains, while the network structure in the module is also similar to that of a series of $[G]_2[M(tdpd)_2(L)_m]$. Fur-

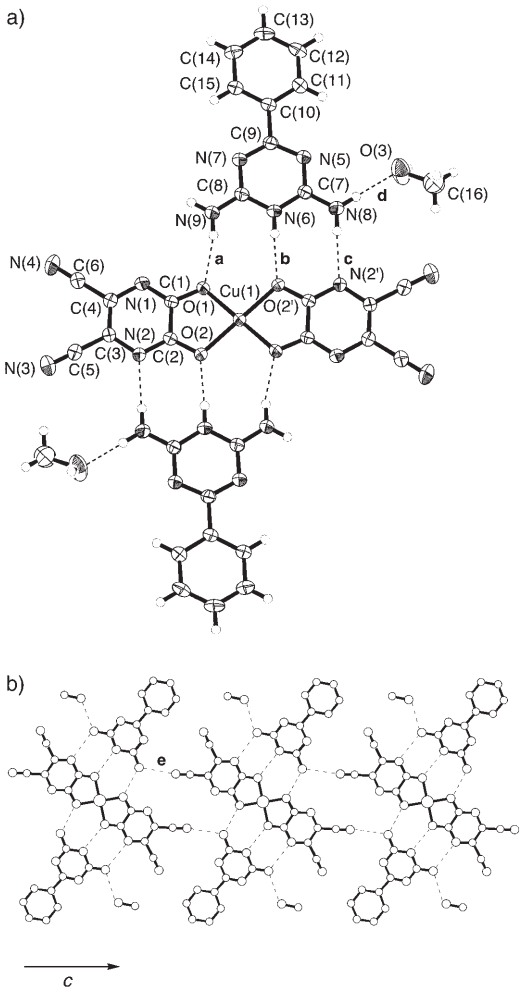

Figure 2. a) ORTEP plot of **3** with labeling scheme and thermal ellipsoids at the 50% probability level for Cu, O, N, and C atoms. Spheres of the hydrogen atoms have been arbitrarily reduced. Hydrogen-bonding parameters: N···N/O, H···N/O distances [Å], N/O–H···N/O angles [°]: **a** 2.840(4), 2.07, 160; **b** 2.820(4), 2.10, 178; **c** 2.942(4), 2.08, 179; **d** 2.854(3), 2.00, 173. b) Part of the hydrogen-bonded chains of molecules present in structure of **3** showing the intermolecular interactions between adjacent modules. Hydrogen-bonding parameters: N···N, H···N distances [Å], N–H···N angles [°]: **e** 3.028(2), 2.17, 176.

thermore, the chains are connected by interchain π–π stacking interactions to create a three-dimensional structure. The distances are 3.37–3.54 Å between the pyrazine rings of the $tdpd^{2-}$ ion and the phenyl rings of the Hbg^{+} ion, and 3.29–3.47 Å between the triazine rings of Hbg^{+} ions.

Although **1**, **2**, and **3** have similar building modules and hydrogen-bonded network structures, there are differences in aggregation mode of the modules: the two-dimensional sheet structures are formed by $[Hbg]_2[M(tdpd)_2(MeOH)_2]$ modules, and the chain structure is formed by $[Hbg]_2[Cu^{II}(tdpd)_2]$ modules. These compounds, prepared under identical conditions, contain metal(II) ions in either a distorted octahedral (**1** and **2**) or square-planar (**3**) geometry, depending on the absence or presence of axially coordinated methanol molecules, and thus the different structures can be described as the results of properties stored in the metal ions. Additionally, compounds **1**–**3** all have the structure in which the AAA/DDD hydrogen-bond interactions link the cations and anions into modules similar to those of the compounds $[Hmel]_2[M(tdpd)_2(H_2O)_2]$,[15] while the assembled structures are different from each other. These results demonstrate that simple modification from $Hmel^{+}$ cation to Hbg^{+} cation can lead to changes in the assembled structures.

Crystal structures of $[Hdamel]_2[Cu^{II}(tdpd)_2]\cdot 2THF$ (4; damel = N^2,N^2-diallylmelamine) and $[Hdhtz]_2[Cu^{II}(tdpd)_2]\cdot 2THF$ (5; dhtz = 2,4-diamino-6-heptyl-1,3,5-triazine): damel and dhtz were chosen as hydrogen-bonding donor molecule for building modules because they have allyl and heptyl groups, respectively, which inhibit π–π stacking between aromatic rings of the modules and change the thermal stability of the crystal.

The structure of $[Hdamel]_2[Cu^{II}(tdpd)_2]\cdot 2THF$ (**4**) consists of mononuclear $[Cu(tdpd)_2]^{2-}$ dianions, $Hdamel^{+}$ cations, and uncoordinated THF molecules. An ORTEP plot of the structure around the copper ion in **4** with the atom numbering scheme is shown in Figure 3a. The structure of **4** shows that the desired coordination and aggregation were achieved: the copper atom is coordinated to the two $tdpd^{2-}$ ions, which are in turn involved in AAA/DDD-type hydrogen bonding with the $Hdamel^{+}$ cations.[23] The square-planar coordination geometry around the copper ion in the monomer involves the four oxygen atoms of the two $tdpd^{2-}$ ions (Cu–O(1), Cu–O(1′) 1.904(3); Cu–O(2), Cu–O(2′) 1.933(2) Å). The three hydrogen-bonding distances between the $tdpd^{2-}$ ion and $Hdamel^{+}$ ion are O(1)···N(9) 2.847(5), O(2′)···N(6) 2.893(4), and N(2′)···N(8) 2.928(5) Å (**a**, **b**, and **c**, respectively, in Figure 3a). The triply hydrogen bonded network of the anionic complex with the $Hdamel^{+}$ cations forms the building module, the structural features of which are also similar to those of a series of $[G]_2[M(tdpd)_2(L)_m]$. A carbon atom on one of the allyl groups and interstitial THF molecules are each disordered over two positions, respectively. The $[Hdamel]_2[Cu(tdpd)_2]$ module is linked to the adjacent modules by additional N(H)···N hydrogen bonds (**e** in Figure 3b) to form one-dimensional chains with structural features similar to those of **3**. The chains exhibit stacking interactions between the $tdpd^{2-}$ ions and the $Hdamel^{+}$ ions on adjacent chains to form two-dimensional layers on the *ab* plane (Figure 3c). The shortest interchain distance of 3.35 Å between the pyrazine rings of the $tdpd^{2-}$ anion and the triazine rings of the $Hdamel^{+}$ cation indicates the existence of a π–π interaction. The interlayer distance, defined as the perpendicular distance between the layers, is 15.42 Å. The allyl groups of the $Hdamel^{+}$ ions adopt a U-shaped conformation and are in a bilayer arrangement. In addition, the $Hdamel^{+}$ ions pair up between layers. The cavities surrounded by the layers are filled with the THF molecules (Figure 3c), linked by N(H)···O hydrogen bonds (**d** in Figure 3a).

The crystal structure of $[Hdhtz]_2[Cu^{II}(tdpd)_2]\cdot 2THF$ (**5**) is similar to that of **4**. The detailed crystallographic procedure

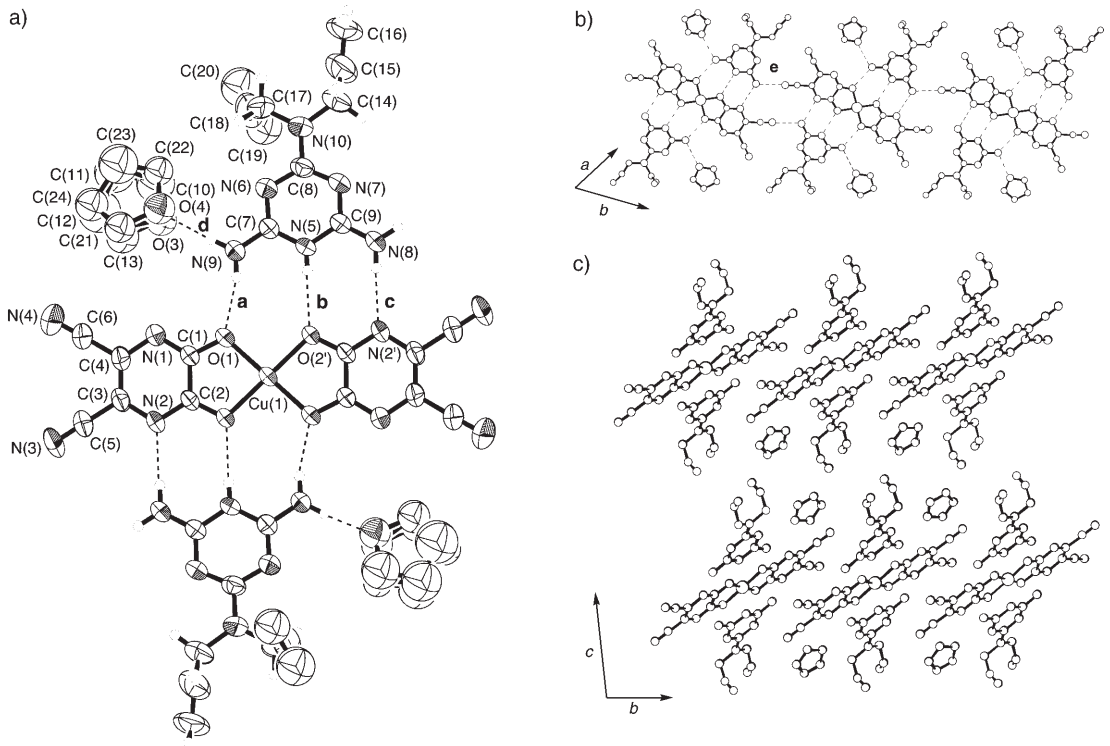

Figure 3. a) ORTEP plot of **4** with labeling scheme and thermal ellipsoids at the 50% probability level for Cu, O, N, and C atoms. Spheres of the hydrogen atoms have been arbitrarily reduced. Hydrogen-bonding parameters: N···N/O, H···N/O distances [Å], N/O–H···N/O angles [°]: **a** 2.847(5), 2.01, 169; **b** 2.893(4), 2.03, 175; **c** 2.928(5), 2.00, 174; **d** 2.87 (av N···O distance). b) Part of the hydrogen-bonded chains of molecules present in structure of **4** showing the intermolecular interactions between adjacent modules. Hydrogen-bonding parameters: N···N, H···N distances [Å], N–H···N angles [°]: **e** 3.043(4), 2.19, 174. c) View of the assembled structure of **4**. The channels are filled with THF molecules.

and data are given in the Supporting Information. X-ray data collection was incomplete due to rapid decomposition of the crystal during measurements. However, we could determine an outline of the sheet structure. The structure of **5** consists of a mononuclear $[Cu(tdpd)_2]^{2-}$ ion, two $Hdhtz^+$ cations, and two interstitial THF molecules. The copper coordination geometry in **5** is distorted square-planar and involves the four oxygen atoms of the two $tdpd^{2-}$ ions. Identical module formation occurs through AAA/DDD interaction. An additional longer hydrogen bond between one of the amino groups of the $Hdhtz^+$ cation and one of the nitrile groups of the $tdpd^{2-}$ ion interlink these modules into one-dimensional chains (Figure 4). The nitrile groups and the pyrazine ring of the $tdpd^{2-}$ ion and the triazine ring of the $Hdhtz^+$ cation extend the one-dimensional chain into a two-dimensional layered structure over the *ab* plane. The interlayer distance is about 15.5 Å. A larger interlayer interdigitation due to the longer heptyl residues is revealed, with the requisite hydrophobic bonds. The interstitial THF molecules form hydrogen bonds to the $Hdhtz^+$ ion.

In **4** and **5**, the hydrogen-bonded layered structures seen in $[Hmel]_2[M(tdpd)_2(H_2O)_2]$ (M^{II} = Ni, Co, Mn, Zn) are complementarily disrupted due to the steric hindrance of the allyl group of $Hdamel^+$ and the heptyl group of $Hdhtz^+$, respectively. Additionally, square-planar geometry of the copper ion eases the stacking interaction between the chains to assemble into two-dimensional structures. Although the

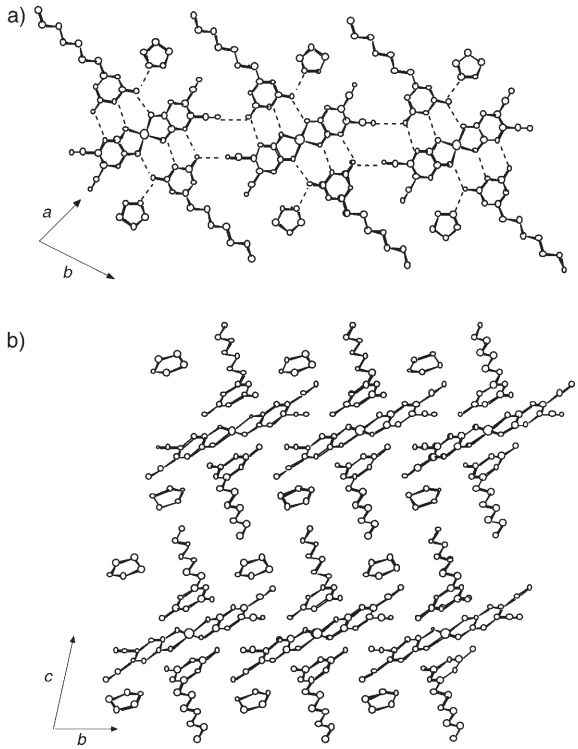

Figure 4. a) Part of the hydrogen-bonded chains of molecules present in the structure of **5** showing the intermolecular interactions between adjacent modules. b) View of the assembled structure of **5**. The channels are filled with THF molecules.

change of the hydrogen-bond donor from bg to damel or dhtz modifies the stacking arrangement in the crystal, the $[G]_2[Cu(tdpd)_2]$ modules are virtually unchanged. Competition between the nonbonding steric interaction and the tendency for a high packing coefficient in the crystal are considered important in determining the assembled structure.

Crystal structure of $(Hdptz)_2[Cu(tdpd)_2]\cdot 2EtOH$ (6; dptz = 2,4-diamino-6-(9-phenanthryl)-1,3,5-triazine: dptz was selected as hydrogen-bonding partner because it has a phenanthryl group with a long conjugated system for introducing optical properties into the hydrogen-bonded module. An ORTEP plot of dptz·EtOH is shown in Figure 5a. The structure of dptz shows the phenanthryl group attached to C(11) as expected. The dihedral angle between the triazine ring and the phenanthryl group is 53°. Double hydrogen bonds between N(1)···N(5) on adjacent molecules form a hydrogen-bonded dimer. The dimers are linked into a corrugated chain connected by interstitial ethanol molecules by hydrogen-bonding interaction (Figure 5b) and, moreover, the chains are connected by π–π stacking interaction between the phenanthryl groups on the nearest-neighbor chains to form a three-dimensional structure.

The structure of **6** consists of mononuclear $[Cu(tdpd)_2]^{2-}$ dianions, $Hdptz^+$ ions, and uncoordinated ethanol molecules. An ORTEP plot of the structure around the copper ion in **6** with the atom numbering scheme is shown in Figure 6a. The structure of **6** shows that the desired coordination and aggregation were achieved: the copper atom is coordinated to two $tdpd^{2-}$ ions, which are in turn involved in AAA/DDD-type hydrogen bonding with $Hdptz^+$ ions. The coordination geometry around the copper ion in the monomer, which involves the four oxygen atoms of $tdpd^{2-}$, is square-planar (Cu–O(1), Cu–O(1′) 1.938(2); Cu–O(2), Cu–O(2′) 1.923(4) Å). The three hydrogen-bonding distances between the $tdpd^{2-}$ ion and $Hdptz^+$ ion are N(1)···N(8) 2.901(5), O(1)···N(5) 2.880(5), and O(2′)···N(9) 2.860(4) Å (**a**, **b**, and **c**, respectively, in Figure 6a). Triple hydrogen bonding of the anionic complex with $Hdptz^+$ cations also forms the building module, as in **1**–**5**. Interestingly, greater planarity of the $Hdptz^+$ ion is found in the module of **6** than in the Hbg^+ ions of **1**–**3**. The $(Hdptz)_2[Cu(tdpd)_2]$ modules and interstitial ethanol molecules are linked to the adjacent modules by additional hydrogen bonds (**e** and **f** in Figure 6b) to form a one-dimensional chain, the structure of which is different from those of **3**–**5** due to the greater steric hindrance of the phenanthryl group: the indirect hydrogen-bonding interaction between the adjacent modules through the ethanol molecules acts as a spacer. Furthermore, the chains are connected by interchain π–π stacking interaction to create a three-dimensional structure. The distances are 3.35(1) [C(21)···C(5)] and 3.413(8) Å [C(22)···(C(3)] between the pyrazine rings of $tdpd^{2-}$ ion and phenyl rings of $Hdptz^+$ ion, and 3.35(1) [C(7)···C(8)] and 3.30(1) Å [C(9)··· (C(17)] between the triazine rings of $Hdptz^+$ ions.

Control of assembled structures: effect of chemical modification of building modules: This series of compounds contains metal ions with octahedral (**1**, **2**, and $[Hmel]_2[M(tdpd)_2(H_2O)_2]$ (M^{II} = Ni, Co, Mn, Zn)) or square-planar (**3**–**6**) geometry, depending on the presence or absence of axially coordinated solvent molecules. All of the compounds have structures in which the AAA/DDD "principal" hydrogen-bond interactions link the cations and anions into similar modules (Figure 7). This work demonstrates that crystal packing can be controlled by using the $[G]_2[M(tdpd)_2(L)_m]$

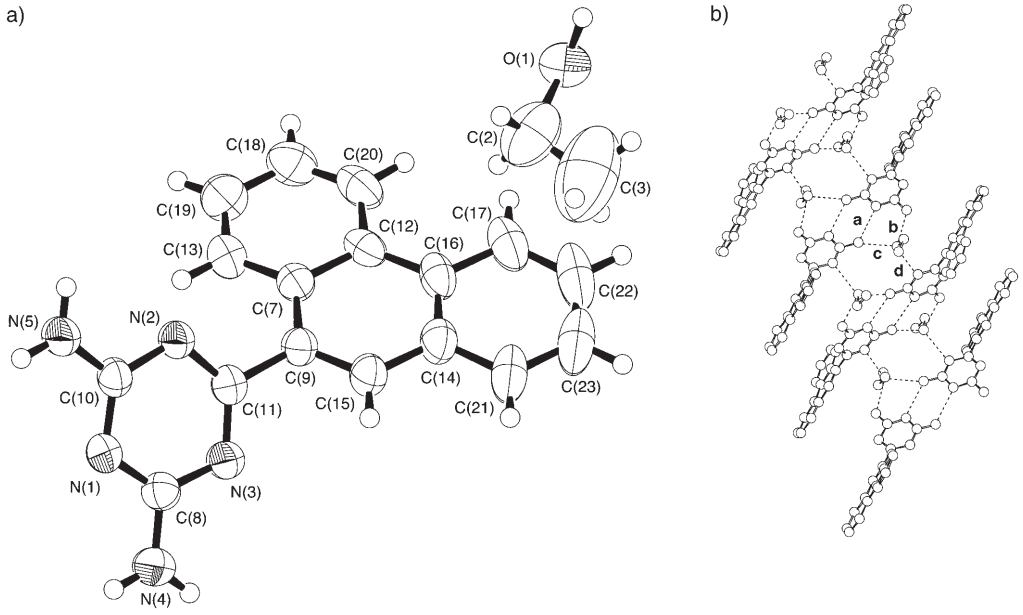

Figure 5. a) ORTEP plot of dptz·EtOH with labeling scheme and thermal ellipsoids at the 50% probability level for O, N, and C atoms. Spheres of the hydrogen atoms have been arbitrarily reduced. b) Part of the hydrogen-bonded chains of molecules present in structure of dptz·EtOH showing the intermolecular hydrogen-bonding interactions. Hydrogen-bond lengths: **a** 3.02, **b** 2.97, **c** 2.91, **d** 2.84 Å.

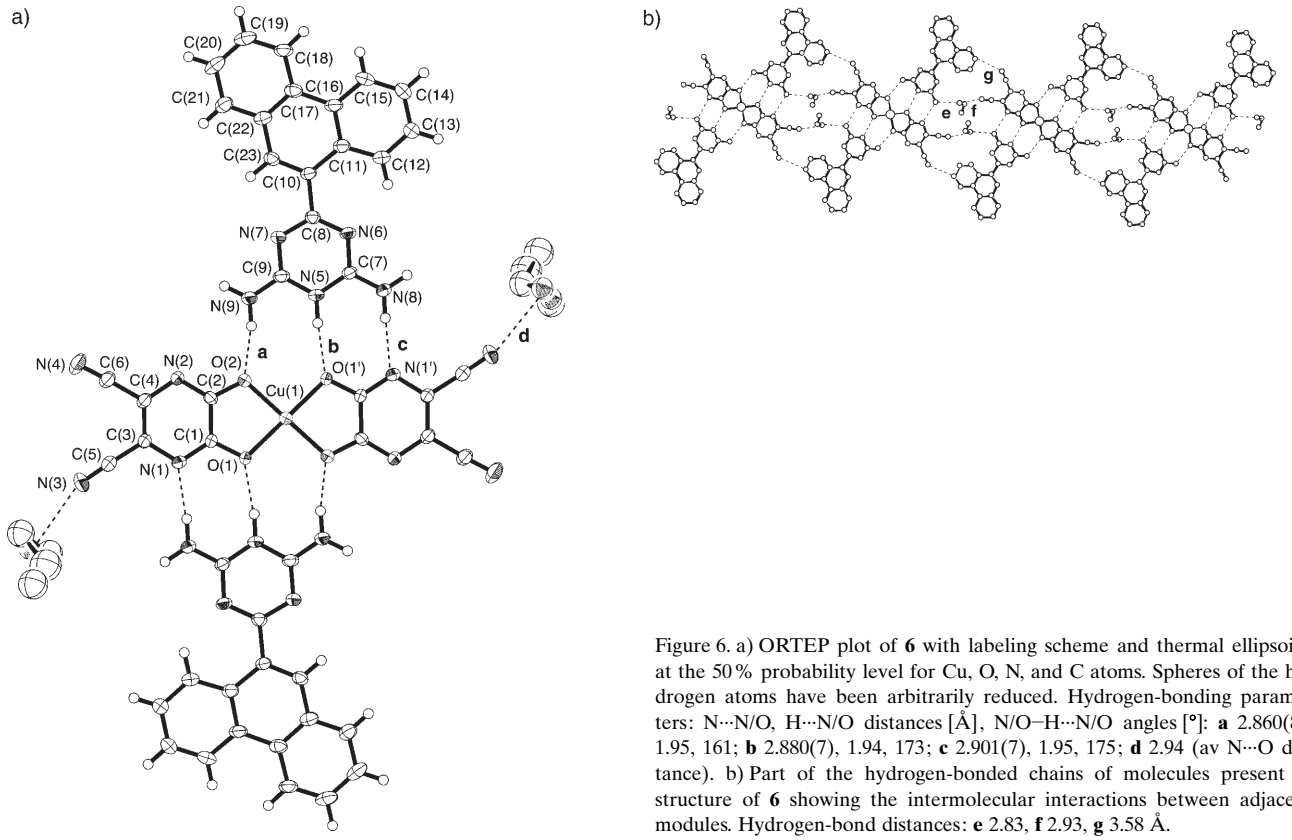

Figure 6. a) ORTEP plot of **6** with labeling scheme and thermal ellipsoids at the 50% probability level for Cu, O, N, and C atoms. Spheres of the hydrogen atoms have been arbitrarily reduced. Hydrogen-bonding parameters: N···N/O, H···N/O distances [Å], N/O–H···N/O angles [°]: **a** 2.860(8), 1.95, 161; **b** 2.880(7), 1.94, 173; **c** 2.901(7), 1.95, 175; **d** 2.94 (av N···O distance). b) Part of the hydrogen-bonded chains of molecules present in structure of **6** showing the intermolecular interactions between adjacent modules. Hydrogen-bond distances: **e** 2.83, **f** 2.93, **g** 3.58 Å.

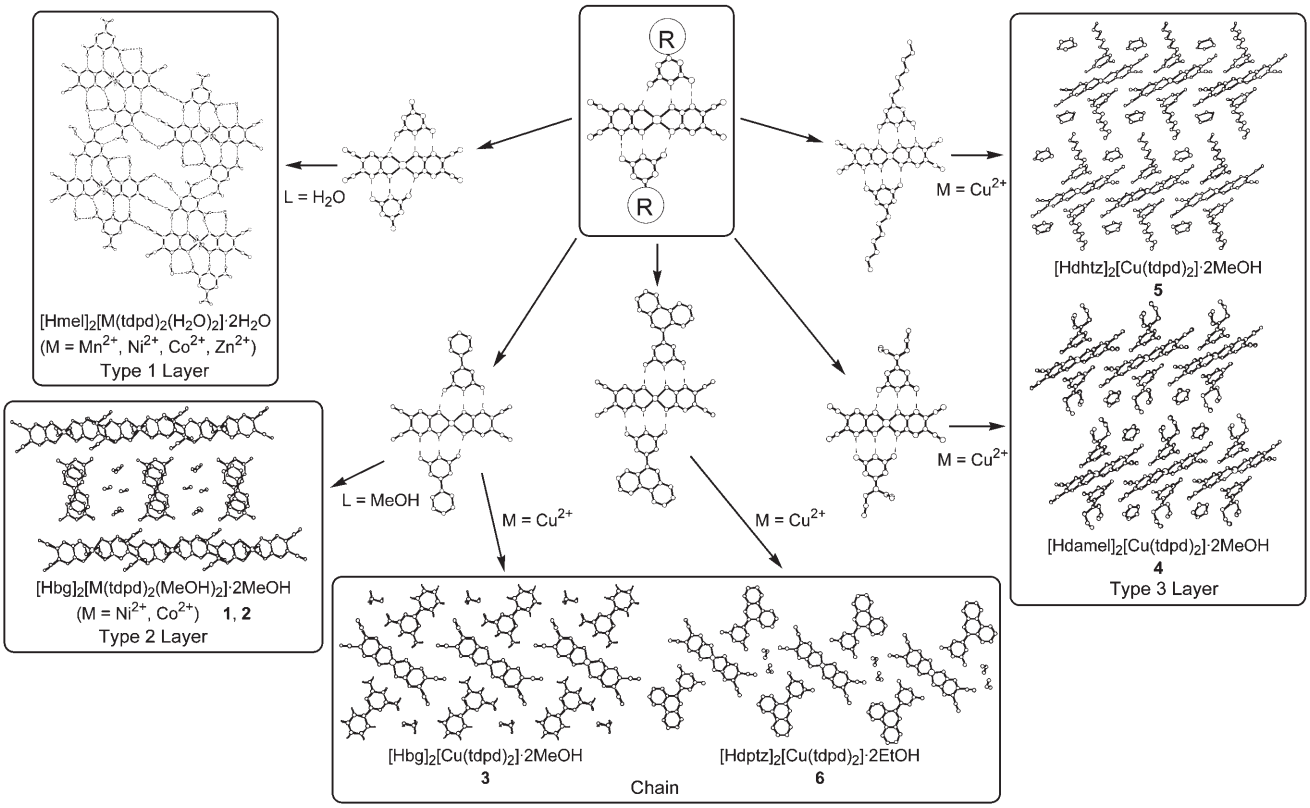

Figure 7. Control of structures: effect of chemical modification of building blocks.

module as a topological director of crystal packing. The $[Hmel]_2[M(tdpd)_2(H_2O)_2]$ modules form a hydrogen-bonded two-dimensional sheet structure (type 1). The robustness of the module suggests that new crystalline materials can be constructed by using this module as the secondary building unit. The $[Hbg]_2[M(tdpd)_2(L)_m]$ modules show that stacking and hydrogen-bonding effects can have dramatic roles in determining crystal packing due to the introduction of the phenyl group at the *exo* site of the module: two-dimensional structure supported by hydrogen bonds between the oxygen atom of methanol and one of the nitrile nitrogen atoms on the $tdpd^{2-}$ ion (type 2), and one-dimensional structure (type 3) supported by hydrogen bonds between the coordinated tdpd ions of adjacent modules. In the cases of **4** and **5**, the type 4 layer structures are formed due to the steric hindrance of functional groups of $Hdamel^+$ ions and the absence of the axially coordinated solvent molecules. The one-dimensional structure of **6** is different from those of **3**–**5** due to the greater steric hindrance of the phenanthryl group: indirect hydrogen bonds are formed between adjacent modules through ethanol molecules that act as spacers.

Although changing the hydrogen-bond donor molecules from bg to damel modifies the stacking arrangement in the crystal, the $[G]_2[M(tdpd)_2(L)_2]$ module is virtually unchanged. It is considered that competition between the nonbonding steric interaction and the tendency for a high packing coefficient in the crystal is important in determining the assembled structure. The assembled structure demonstrates that simple modifications in the structure of the melamine or the modules can lead to changes in crystal architecture that can be rationalized by steric arguments and a high packing coefficient in the crystal. By varying the steric demands of substituents around the hydrogen-bonded components, it is expected to be possible to select hydrogen-bonded assemblies in the solid state.

Thermal properties of $[Hdamel]_2[Cu^{II}(tdpd)_2]\cdot 2THF$ (4): Thermogravimetry (TG) and differential scanning calorimetry (DSC) were carried out under a nitrogen atmosphere. The combined TGA/DTA curves for **4** are shown in Figure 8a. The TG analysis is consistent with the crystallographic observations. Liberation of THF molecules occurs between 330 and 470 K, and thus the species obtained from **4** in the intermediate range of 470–570 K is assigned to the desolvated compound $[Hdamel]_2[Cu(tdpd)_2]$. Interestingly, this process shows that interstitial THF molecules are released at a temperature above the boiling point of THF, indicative of the presence of strong hydrogen-bonding interaction and steric hindrance of the allyl group of the $Hdamel^+$ ions.

On the other hand, DSC traces of **4** show that a thermal hysteresis occurs around 155 K, the temperature of which is lower than the melting point of THF, while free damel has no thermal anomalies in this temperature region (Figure 8b). As the temperature is lowered, an exothermic peak is observed at 153 K and the endothermic peak occurs at 159 K on warming. The enthalpy and entropy variations are

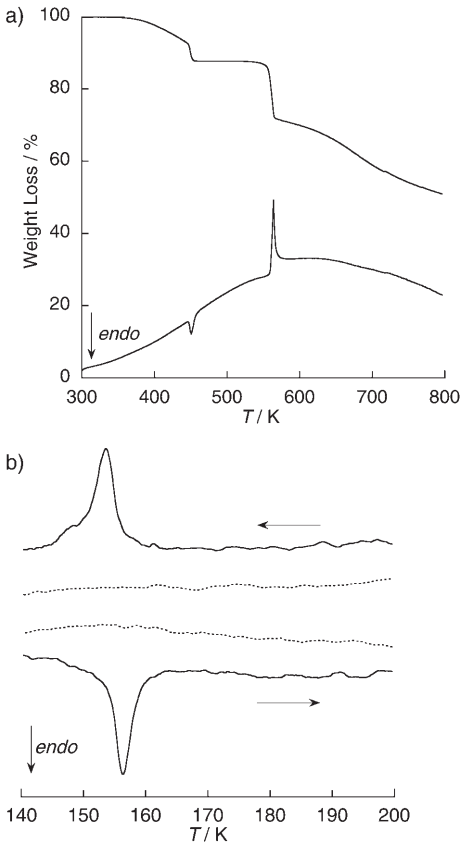

Figure 8. a) TG analysis data for **4**. b) DSC traces of **4** (solid lines) and damel (dotted lines).

$\Delta H = 1.0\ kJ\,mol^{-1}$ and $\Delta S = 6.4\ J\,mol^{-1}K^{-1}$. In the crystal structure at 295 K, one of the allyl groups of the $Hdamel^+$ ions and THF molecules are each disordered over two positions. Moreover, the cell volume of **4** at 140 K is three times larger than that at 295 K, and the crystal structure at lower temperature shows two kinds of units built up of the modules and two adjacent THF molecules in the unit cell with $Z = 3$ (type 1 and 2 units in Figure S-2, Supporting Information). Thus, the peak in the DSC trace is attributed to the structural phase transition caused by relocation of the allyl groups of the $Hdamel^+$ ions with THF molecules: the structural phase transition detected by single-crystal X-ray diffraction is thought to be dynamical, since there are no other thermal anomalies, and **4** attains thermal equilibrium in two phases. In such a case, the structural disorder contributes to entropy according to Boltzman's relation, $\Delta S = xR\ln n$, where x is the population of the disordered unit in the unit cell, n the number of available microstates per formula unit, and R the gas constant. If both of the THF molecules and the allyl groups are independently disordered in the high-temperature phase, contribution of the unit to entropy is $R\ln(2^2\times 2^2) = 23.1\ J\,mol^{-1}K^{-1}$. On the other hand, two-thirds of the units show disorder at both of the allyl groups and interstitial THF molecules (type 1), and one-third of the units show disorder only at the THF molecules (type 2) for the low-temperature phase. If the THF molecules and the allyl

groups are independently disordered in the type 1 unit and the motion of the THF molecules in the type 2 unit is synchronized, the contribution of the unit to entropy is $1/3\,R\ln(2^4\times2\times2^4)=17.3\,\mathrm{J\,mol^{-1}\,K^{-1}}$ for the low-temperature phase.[24] The difference is $5.8\,\mathrm{J\,mol^{-1}\,K^{-1}}$, which is comparable to the observed difference.

The powder X-ray diffraction (PXRD) pattern of the desolvated compound is compared with those of **4** in Figure 9.

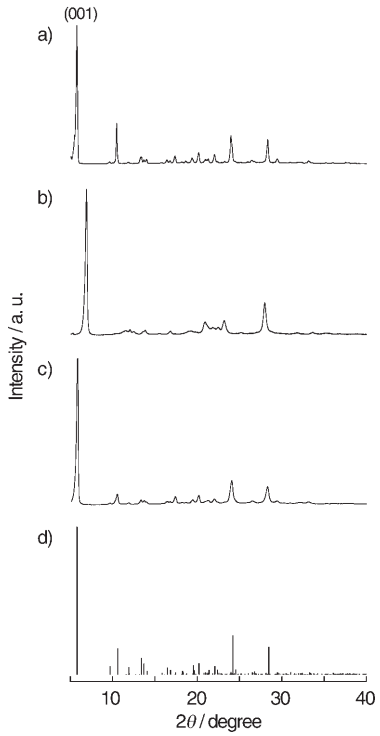

Figure 9. Comparison of the powder X-ray diffraction patterns of **4**. a) Original crystal. b) Solid heated at 200 °C. c) Solid obtained by exposing b) to THF vapor. d) simulated pattern obtained from the crystal structure of **4**.

The solid obtained by heating crystals of **4** to 200 °C shows PXRD patterns in which the positions and intensities of some lines are changed relative to those of the original sample, while the crystal morphology of **4** is maintained through the heating process. However, when this desolvated solid is exposed to saturated THF vapor, the same PXRD pattern as that of the original crystals is regenerated. The original solvated crystal structure of **4** is regained, and this demonstrates the reversibility of the solvent-induced structural transformation. The weight loss behavior of compound **4** before and after exposure were in agreement with each other. These results show that **4** is sustained entirely by noncovalent interactions and has the ability to intercalate guest molecules due to the two-dimensional structure and its flexibility.

Absorption spectra and photophysical properties of 6: The electronic absorption spectra of dptz and **6** are shown in Figure 10a. Free dptz shows absorption bands at 258 and

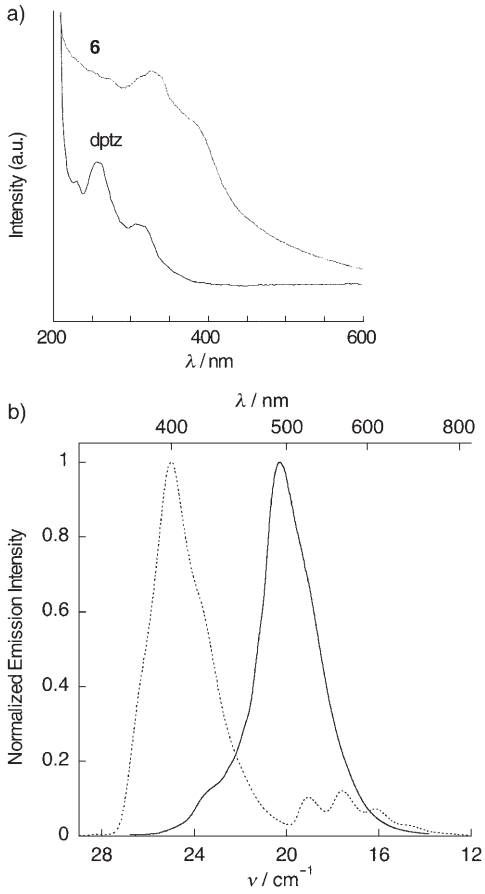

Figure 10. a) Electronic absorption spectra of **6** and dptz in KBr. b) Emission spectra observed for dptz (dotted line) and **6** (solid line) in the solid state at 77 K.

315 nm, while the electronic spectrum of **6** exhibits bands at 330 and 385 nm. At 77 K, dptz displays intense photoluminescence with an emission maximum at 400 nm on excitation at 355 nm in the solid state (Figure 10b). Compared with fluorescence of unsubstituted phenanthrene [$\tilde{\nu}=33\,000\,\mathrm{cm^{-1}}$ (300 nm)],[25] the emission of dptz is structureless and considerably red shifted. Excitation of a crystalline sample of **6** at 77 K gives weak photoluminescence with an emission maximum at 500 nm. Although the intensity around the high-energy side of the spectra varied slightly in each crystal sample, probably due to the presence of small amounts of emissive impurities, the shape of the entire spectrum seems to be almost the same as that of dptz. Calculation of excitation energies at the TD-B3LYP level using the X-ray structure of dptz indicates that the absorption band at 315 nm is assigned to the transition to an excited state formed by configurational mixing between $\pi\pi^*$ in the phenanthryl moiety and charge transfer (CT) from the phenanthryl to the triazole moiety (2^1A_u, Table S-1, Supporting Information). The intense and structureless emission is presumed to originate from the 2^1A_u state having CT character. On the other hand, both the absorption and emission peak energies for **6** are about $5000\,\mathrm{cm^{-1}}$ lower than those for dptz. It is most likely that the CT states in **6** are considera-

bly stabilized by protonation on the central nitrogen atom of the $Hdptz^+$ ion, and thereby the CT absorption band and the corresponding emission are shifted to the lower energy region. The TD-B3LYP calculation using the X-ray structure of dptz also supports this idea: both the absorption bands at 330 and 385 nm are assigned to CT from the phenanthryl to the triazole moiety (6^2A_u and 8^2A_u, Table S-2).

A phosphorescence spectrum with a well-resolved vibrational structure was observed for dptz in a lower energy region of $(14–20)\times10^3\ cm^{-1}$. The emission energy and the vibrational structure are similar to those of the phosphorescence of phenanthrene (ca. $21.7\times10^3\ cm^{-1}$).[26]

The emission lifetime of dptz at 77 K was 29 ns, whereas that of **6** was only 70 ps. The remarkably short lifetime of the CT state in **6** is presumably ascribed to quenching via electron transfer to the copper(II) ion or energy transfer to a ligand-to-metal CT state in the copper(II)–tdpd moiety through the triple hydrogen bonds.

Conclusion

The hydrogen-bonding interaction plays an important role in determining the structure of assembled complexes. The ligand $tdpd^{2-}$ ion fulfils its bifunctional role by generating a transition metal complex as part of a multidimensional cocrystallized network, self-assembled by a combination of coordination and hydrogen-bond formation. Complexes $[M(tdpd)_2(L)_m]^{2-}$ with AAA hydrogen-bonding recognition sites have been synthesized and shown to form $[G]_2[M(tdpd)_2(L)_m]$ modules with protonated melamine or its analogues having a DDD motif. These modules of compounds **1**–**6**, to the best of our knowledge, are the first examples of an AAA/DDD system in self-assembled complexes. While the structure of the $[G]_2[M(tdpd)_2(L)_m]$ modules among ten compounds are similar, the differences in hydrogen-bonding capability result in markedly different packing configurations for assembled structures (Figure 7). These differences are brought about by the different steric constraints imposed by the hydrogen-bond donor molecules, as well as by the interaction among the hydrogen-bond donor molecules themselves and the absence or presence of axially coordinated molecules. Therefore, the utility of this modular approach at the supramolecular level through the design of mixed and composite crystals is a successful procedure to prepare new types of metal-assembled complexes. Advances in their design will depend on crystal engineering that involves the development of convenient synthetic strategies leading to a better control of the supramolecular structure of the materials.

Experimental Section

$[Hbg]_2[Ni^{II}(tdpd)_2(MeOH)_2]\cdot4MeOH$ (1): An aqueous solution (10 mL) of nickel(II) chloride hexahydrate (0.5×10^{-5} mol) and H_2tdpd (1×10^{-5} mol) was transferred to a glass tube, and a methanolic solution (10 mL) of benzoguanamine (bg) (1×10^{-5} mol) poured into the tube without mixing the two solutions at room temperature. Light green plate crystals began to form over three weeks; yield 50%. One of these crystals was used for X-ray crystallography. Elemental analysis (%) calcd for $C_{36}H_{44}NiN_{18}O_{10}$: C 45.63, H 4.68, N 26.61; found: C 45.73, H 4.73, N 26.40.

$[Hbg]_2[Co^{II}(tdpd)_2(MeOH)_2]\cdot4MeOH$ (2): Compound **2** was synthesized from cobalt(II) acetate tetrahydrate by a procedure similar to that employed for **1**. Light orange plate crystals began to form over a month; yield 50%. One of these crystals was used for X-ray crystallography. Elemental analysis (%) calcd for $C_{36}H_{44}CoN_{18}O_{10}$: C 45.62, H 4.68, N 26.60; found: C 45.83, H 4.80, N 26.30.

$[Hbg]_2[Cu^{II}(tdpd)_2]\cdot2MeOH$ (3): Compound **3** was synthesized from copper(II) sulfate pentahydrate by a procedure similar to that employed for **1**. Green plate crystals began to form over three weeks; yield 60%. One of these crystals was used for X-ray crystallography. Physical measurements were conducted on a polycrystalline powder that was synthesized as follows: An aqueous solution (100 mL) of copper(II) sulfate pentahydrate (0.05 mmol) and H_2tdpd (0.1 mmol) was added dropwise to an methanolic solution (100 mL)of bg (0.1 mmol). When the mixture was stirred, a light green powder appeared immediately. Elemental analysis (%) calcd for $C_{32}H_{28}CuN_{18}O_6$: C 46.63, H 3.42, N 30.59; found: C 46.39, H 3.25, N 30.62.

$[Hdamel]_2[Cu^{II}(tdpd)_2]\cdot2THF$ (4): A THF solution (10 mL) of copper(II) trifluoroacetate (0.5×10^{-5} mol) and H_2tdpd (1×10^{-5} mol) was transferred to a glass tube, and an ethanolic solution (10 mL) of N^2,N^2-diallylmelamine (damel) (1×10^{-5} mol) poured into the tube without mixing the two solutions at room temperature. Green plate crystals began to form over a month; yield 50%. One of these crystals was used for X-ray crystallography. Physical measurements were conducted on a polycrystalline powder that was synthesized as follows: A THF solution (100 mL) of copper(II) trifluoroacetate (0.05 mmol) and H_2tdpd (0.1 mmol) was added dropwise to an ethanolic solution (100 mL) of damel (1×10^{-4} mol). When the mixture was stirred, a light green powder appeared immediately. Elemental analysis (%) calcd for $C_{38}H_{46}CuN_{20}O_6$: C 48.43, H 4.92, N 29.72; found: C 48.48, H 4.87, N 29.86.

$[Hdhtz]_2[Cu^{II}(tdpd)_2]\cdot2THF$ (5): 2,4-Diamino-6-heptyl-1,3,5-triazine (dhtz) was synthesized first. Octanenitrile (12.5 g, 0.1 mol) was heated under reflux overnight with dicyanodiamide (8.4 g, 0.1 mol) and potassium hydroxide (1.7 g, 0.03 mol) in dry 2-propanol (120 mL). After cooling to ambient temperature, large colorless crystals were obtained; yield 70%; m.p. 166.7°C; ^1H NMR ([D$_6$]DMSO): $\delta=5.71$ (br, 4H), 1.46 (t, 2H), 0.77 (m, 2H), 0.43 (m, 8H), 0.03 ppm (t, 3H); IR (KBr): $\tilde{\nu}=3489$, 3304, 3191, 3107, 2958, 2927, 2852, 1674, 1636, 1548, 1457, 1404 cm^{-1}; Elemental analysis (%) calcd for $C_{10}H_{19}N_5$: C 57.39, H 9.15, N 33.46; found: C 57.47, H 9.12, N 33.33. A THF solution (10 mL) of copper(II) trifluoroacetate (0.5×10^{-5} mol) and H_2tdpd (10^{-5} mol) was transferred to a glass tube, and an ethanolic solution (10 mL) of dhtz (10^{-5} mol) poured into the tube without mixing the two solutions at room temperature. Green plate crystals began to form over a month; yield 50%. One of these crystals was used for X-ray crystallography. Elemental analysis (%) calcd for $C_{40}H_{56}CuN_{18}O_6$: C 50.65, H 5.95, N 26.58; found: C 50.16, H 5.73, N 26.22.

$(Hdptz)_2[Cu(tdpd)_2]\cdot2EtOH$ (6): 2,4-Diamino-6-(9-phenanthryl)-1,3,5-triazine (dptz) was synthesized first. The following procedure, adapted from the literature, was used to prepare the malamine analogues described in this paper. 9-Cyanophenanthrene (20.3 g, 0.1 mol) was heated under reflux overnight with dicyanodiamide (8.4 g, 0.1 mol) and potassium hydroxide (1.7 g, 0.03 mol) in dry 2-propanol (120 mL). After the mixture was allowed to cool to ambient temperature, a white precipitate was obtained and recrystallized from ethanol; yield 70%; m.p. 259.9°C; ^1H NMR ([D$_6$]DMSO): $\delta=8.13$ (d, 2H), 7.59 (d, 1H), 7.36 (s, 1H), 7.16 (s, 1H), 7.06 (m, 4H), 6.07 ppm (br, 4H); IR (KBr): $\tilde{\nu}$3488, 3378, 3289, 3191, 3108, 3070, 1642, 1621, 1523, 1447, 1407, 1369 cm^{-1}. An aqueous solution (1 mL) of copper(II) acetate monohydrate (5 mmol L^{-1}) and H_2tdpd (5 mmol L^{-1}) was transferred to a glass tube, and an ethanolic solution of dptz (5 mmol L^{-1}) poured into the tube without mixing the two solutions. Green plate crystals began to form over three weeks; yield

50%. One of these crystals was used for X-ray crystallography. Elemental analysis (%) calcd for $C_{50}H_{40}Cu_1N_{18}O_6$: C 57.06, H 3.83, N 23.95; found: C 57.16, H 3.74, N 24.22.

Physical measurements: IR spectra were measured on a JASCO FT/IR-410 spectrophotometer in KBr disks. UV and visible spectra were measured on a JASCO V-570 spectrometer. Powder X-ray diffraction data were collected on a Rigaku RINT 2000 diffractometer by using $Cu_{K\alpha}$ radiation. Thermal gravimetric (TG) analysis and differential scanning calorimetry (DSC) were carried out with a Seiko Instruments Inc. SSC5200 thermo-analyzer in a nitrogen atmosphere (heating rates: 10 K min^{-1} for TG, 5 K min^{-1} for DSC). Electrospray ionization mass (ESI-MS) spectra were recorded a Perkin Elmer API-III spectrometer. Steady-state emission spectra were recorded by a grading monochromator (Triax 1900) with a CCD image sensor (Hamamatsu S7031). The spectral sensitivity of the spectrofluorometer was corrected with a bromine lamp (Ushio IPD 100 V 500WCS). A sample in a cylindrical quartz cell (∅ 2 mm) was excited with an Nd^{3+}:YAG laser (355 nm, 2 mW, pulse width 1 ns, 10 kHz repetition rate, NANOLASE). The spectra at 77 K were measured in a liquid-nitrogen Dewar. The emission intensities in all the spectra are relative numbers of quanta at each frequency. The emission lifetimes of **6** and dptz were measured by using a time-correlated single-photon counting system.[18] The second harmonic (400 nm, 10–50 mW, 80 MHz repetition rate) of a mode-locked Ti^{3+}:saphire laser (Tsunami, Spectra Physics) was used for excitation of a sample solution in the cylindrical cell. The in-

Table 1. Crystallographic data for **1**–**4**, **6**, and dptz·EtOH.

Compound	[Hbg]$_2$[Ni(tdpd)$_2$(MeOH)$_2$]·2MeOH (**1**)	[Hbg]$_2$[Co(tdpd)$_2$(MeOH)$_2$]·2MeOH (**2**)	[Hbg]$_2$[Cu(tdpd)$_2$]·2MeOH (**3**)
empirical formula	$Ni_1C_{36}N_{18}O_{10}H_{44}$	$Co_1C_{36}N_{18}O_{10}H_{44}$	$CuC_{32}N_{18}O_6H_{28}$
formula weight	947.60	947.82	824.26
crystal dimensions [mm]	0.30×0.10×0.10	0.30×0.10×0.10	0.20×0.10×0.10
crystal system	triclinic	triclinic	triclinic
space group	$P\bar{1}$ (no. 2)	$P\bar{1}$ (no. 2)	$P\bar{1}$ (no. 2)
a [Å]	8.3611(5)	8.3874(3)	7.273 7.273(3)
b [Å]	10.3348(7)	10.4121(4)	9.991(3)
c [Å]	14.224(1)	14.2168(5)	13.099(3)
α [°]	68.704(3)	68.741(3)	106.83(2)
β [°]	80.930(3)	80.787(3)	94.68(3)
γ [°]	80.382(1)	80.634(1)	95.57(3)
V [Å^3]	1122.8(1)	1134.73(7)	900.7(5)
Z	1	1	1
ρ_{calcd} [g cm^{-3}]	1.401	1.387	1.520
F(000)	494	493	423.00
linear absorption coefficient [cm^{-1}]	5.07 (MoKα)	4.52 (MoKα)	6.79 (MoKα)
diffractometer	Rigaku RAXIS-RAPID	Rigaku RAXIS-RAPID	Mac Science MXC3
$2\theta_{max}$ [°]	54.9	55	55
total reflections measured	7861	10450	4598
unique reflections	4990	4925	4598
reflections used	4990	4925	4132
variables	296	296	260
R	0.044	0.051	0.050
wR_2	0.129	0.140	0.126
GOF	1.07	1.08	0.973

Compound	[Hdamel]$_2$[Cu(tdpd)$_2$]·2THF (**4**)	[Hdptz]$_2$[Cu(tdpd)$_2$]·2EtOH (**6**)	dptz·EtOH
empirical formula	$CuC_{38}N_{20}O_6H_{46}$	$CuC_{50}N_{18}O_6H_{40}$	$C_{19}N_5O_1H_{19}$
formula weight	942.46	1052.53	333.39
crystal dimensions [mm]	0.30×0.20×0.10	0.20×0.20×0.05	0.20×0.20×0.20
crystal system	triclinic	triclinic	monoclinic
space group	$P\bar{1}$ (no. 2)	$P\bar{1}$ (no. 2)	$C2/c$ (no. 15)
a [Å]	8.153(1)	9.01(3)	16.415(6)
b [Å]	10.023(2)	10.83(3)	15.497(6)
c [Å]	15.421(2)	13.00(3)	13.455(6)
α [°]	96.44(1)	96.05(5)	90
β [°]	92.29(1)	93.26(4)	94.274(11)
γ [°]	113.42(1)	110.73(4)	90
V [Å^3]	1144.1(3)	1173(5)	3413(2)
Z	1	1	8
ρ_{calcd} [g cm^{-3}]	1.405	1.489	1.298
F(000)	491	537	1408
linear absorption coefficient [cm^{-1}]	5.45 (MoKα)	5.39 (MoKα)	0.85 (MoKα)
diffractometer	Mac Science MXC3	Rigaku/MSC Mercury CCD	Rigaku/MSC Mercury CCD
$2\theta_{max}$ [°]	55	53	55
total reflections measured	5719	10226	17588
unique reflections	5235	5032	3524
reflections used	3384	4836	2367
variables	290	337	230
R	0.070	0.075	0.088
wR_2	0.207	0.181	0.244
GOF	1.01	1.27	1.20

strumental response function of the system was 35 ps at the full width at half-maximum. For a crystalline sample of dptz, lifetimes were measured with excitation at 355 nm by using the nanosecond pulsed laser.

Crystallographic data collection and structure refinement: A suitable crystal was chosen and mounted on a glass fiber with epoxy resin. Data collections for compounds **3** and **4** were carried out on a Mac Science MXC3 with graphite-monochromated $Mo_{K\alpha}$ radiation. Data collections for compounds **1** and **2** were carried out on a Rigaku RAXIS-RAPID with graphite-monochromated $Mo_{K\alpha}$ radiation. Data collections for compounds **5** and **6** were carried out on a Rigaku/MSC Mercury CCD diffractometer with graphite-monochromated $Mo_{K\alpha}$ radiation. Crystallographic data are given in Table 1. The structures were solved by direct methods (Rigaku CrystalStructure crystallographic software package of Molecular Structure Corporation) and refined with full-matrix least-squares technique (SHELXL-97).[19]

CCDC-268469 (**1**), CCDC-268470 (**2**), CCDC-268471 (**3**), CCDC-268472 (**4**), CCDC-268473 (**5**), CCDC-268474 (**6**), CCDC-268475 (dptz·EtOH), and CCDC-268476 (**4**, 140 K) contain the supplementary crystallographic data for this paper. These data can be obtained free of charge from the Cambridge Crystallographic Data Centre via www.ccdc.cam.ac.uk/data_request/cif.

Computational chemistry: Electronic structures and excitation energies were calculated by DFT and time-dependent DFT (TDDFT) with Gaussian 98.[20] The Dunning–Hay split-valence double-zeta basis functions with one polarization function were used for C, H, and N atoms. For Cu atoms, Hay–Wadt double-zeta basis function with Los Alamos relativistic effective core potential was used. In all the DFT calculations, Becke's three-parameter hybrid functional B3LYP was used. MOLEKEL was used to draw molecular orbitals.[21]

Acknowledgement

This research was supported by a Grant-in-Aid for Scientific Research (No. 15550050) and by a Grant-in-Aid for Scientific Research on Priority Areas (No. 434) from the Ministry of Education, Culture, Sports, Science, and Technology of Japan.

[1] a) J.-M. Lehn, *Supramolecular Chemistry; Concepts and Perspectives*, VCH, Weinheim, **1995**; b) J. L. Atwood, J. W. Steed, *Encyclopedia of Supramolecular Chemistry*, Marcel Dekker, New York, **2004**; c) J. W. Steed, J. L. Atwood, *Supramolecular Chemistry*, Wiley, Chichester, **2000**; d) M. M. Mammen, S.-K. Choi, G. M. Whitesides, *Angew. Chem.* **1998**, *110*, 2908; *Angew. Chem. Int. Ed.* **1998**, *37*, 2754; e) D. S. Lawrence, T. Jiang, M. Levett, *Chem. Rev.* **1995**, *95*, 2229; f) M. C. Etter, *Acc. Chem. Res.* **1990**, *23*, 120.

[2] a) J. D. Dunitz, A. Gavezzotti, *Angew. Chem.* **2005**, *117*, 1796; *Angew. Chem. Int. Ed.* **2005**, *44*, 1766; b) S. Kitagawa, K. Uemura, *Chem. Soc. Rev.* **2005**, *34*, 109; c) E. A. Meyer, R. K. Castellano, F. Diederich, *Angew. Chem.* **2003**, *115*, 1244; *Angew. Chem. Int. Ed.* **2003**, *42*, 1210; d) T. Steiner, *Angew. Chem.* **2002**, *114*, 50; *Angew. Chem. Int. Ed.* **2002**, *41*, 48; e) D. C. Sherrington, K. A. Taskinen, *Chem. Soc. Rev.* **2001**, *30*, 83.

[3] a) G. R. Desiraju, T. R. Steiner, *The Weak Hydrogen Bond in Structural Chemistry and Biology*, Oxford University Press, Oxford, **1999**; b) G. Cooke, V. M. Rotello, *Chem. Soc. Rev.* **2002**, *31*, 275; c) J. A. R. P. Sharma, G. R. Desiraju, *Cryst. Growth Des.* **2002**, *2*, 93.

[4] a) H.-C. Chou, C.-H. Hsu, Y.-M. Cheng, C.-C. Cheng, H.-W. Liu, S.-C. Pu, P.-T. Chou, *J. Am. Chem. Soc.* **2004**, *126*, 1650; b) M. D. Ward, *Chem. Soc. Rev.* **1997**, *26*, 365.

[5] J. L. Sessler, M. Sathiosatham, C. T. Brown, T. A. Rhodes, G. Wiederrecht, *J. Am. Chem. Soc.* **2001**, *123*, 3655.

[6] R. A. Marcus, *J. Phys. Chem. B* **1998**, *102*, 10071.

[7] a) E. B. Babini, I. Borsari, M. Capozzi, F. Luchinat, C. Zhang, X. Moura, G. L. C. Kurnikov, I. V. Beratan, D. N. Adrian, P. Di Bilio, A. J. Winkler, J. R. H. B. Gray, *J. Am. Chem. Soc.* **2000**, *122*, 4532; b) J. M. Nocek, J. S. Zhou, S. De Forest, S. Priyadarshy, D. N. Beratan, J. N. Onuchic, B. M. Hoffman, *Chem. Rev.* **1996**, *96*, 2459.

[8] M. A. Smitha, E. Prasad, K. R. Gopidas, *J. Am. Chem. Soc.* **2001**, *123*, 1159.

[9] a) C. Janiak, *Dalton Trans.* **2003**, 2781; b) R. Kitaura, S. Kitagawa, Y. Kubota, T. C. Kobayashi, K. Kindo, Y. Mita, A. Matsuo, M. Kobayashi, H.-C. Chang, T. C. Ozawa, M. Suzuki, M. Sakata, M. Takata, *Science* **2002**, *298*, 2358; c) S. Kitagawa, M. Kondo, *Bull. Chem. Soc. Jpn.* **1998**, *71*, 1739; d) S. Kitagawa, R. Kitaura, S. Noro, *Angew. Chem.* **2004**, *116*, 2388; *Angew. Chem. Int. Ed.* **2004**, *43*, 2334; e) H. K. Chae, D. Y. Siberio-Perez, J. Kim, Y. Go, M. Eddaoudi, A. J. Matzger, M. O'Keeffe, O. M. Yaghi, *Nature* **2004**, *427*, 523; f) M. Eddaoudi, D. B. Moler, H. Li, B. Chen, T. M. Reineke, M. O'Keeffe, O. M. Yaghi, *Acc. Chem. Res.* **2001**, *34*, 319; g) N. L. Rosi, J. Kim, M. Eddaoudi, B. Chen, M. O'Keeffe, O. M. Yaghi, *J. Am. Chem. Soc.* **2005**, *127*, 1504; h) O. Sato, *Acc. Chem. Res.* **2003**, *36*, 692; i) O. Sato, T. Kawakami, M. Kimura, S. Hishiya, S. Kubo, Y. Einaga, *J. Am. Chem. Soc.* **2004**, *126*, 13176; j) R. Clerac, H. Miyasaka, M. Yamashita, C. Coulon, *J. Am. Chem. Soc.* **2002**, *124*, 12837; k) H. Kishida, H. Matsuzaki, H. Okamoto, T. Manabe, M. Yamashita, Y. Taguchi, Y. Tokura, *Nature* **2000**, *405*, 929; l) E. Coronado, J. R. Galán-Mascarós, C. J. Gómez-García, V. Laukhin, *Nature* **2000**, *408*, 447; m) A. Cornia, A. C. Fabretti, P. Garrisi, C. Mortal, D. Bonacchi, D. Gatteschi, R. Sessoli, L. Sorace, W. Wernsdorfer, A.-L. Barra, *Angew. Chem.* **2004**, *116*, 1156; *Angew. Chem. Int. Ed.* **2004**, *43*, 1136; n) D. Gatteschi, R. Sessoli, *Angew. Chem.* **2003**, *115*, 278; *Angew. Chem. Int. Ed.* **2003**, *42*, 268; o) M. Fujita, N. Fujita, K. Ogura, K. Yamaguchi, *Nature* **1999**, *400*, 52; p) O. Ohmori, M. Kawano, M. Fujita, *Angew. Chem.* **2005**, *117*, 1998; *Angew. Chem. Int. Ed.* **2005**, *44*, 1962.

[10] S. Kitagawa, S. Kawata, *Coord. Chem. Rev.* **2002**, *224*, 11.

[11] a) K. Yamada, S. Yagishita, H. Tanaka, K. Tohyama, K. Adachi, S. Kaizaki, H. Kumagai, K. Inoue, R. Kitaura, H.-C. Chang, S. Kitagawa, S. Kawata, *Chem. Eur. J.* **2004**, *10*, 2648; b) K. Nagayoshi, M. K. Kabir, H. Tobita, K. Honda, M. Kawahara, M. Katada, K. Adachi, H. Nishikawa, I. Ikemoto, H. Kumagai, Y. Hosokoshi, K. Inoue, S. Kitagawa, S. Kawata, *J. Am. Chem. Soc.* **2003**, *125*, 221; c) A. M. Beatty, *CrystEngComm* **2001**, 51 ; d) D. Braga, F. Grepioni, *Angew. Chem.* **2004**, *116*, 4092; *Angew. Chem. Int. Ed.* **2004**, *43*, 4002.

[12] M. Kawahara, M. K. Kabir, K. Yamada, K. Adachi, H. Kumagai, Y. Narumi, K. Kindo, S. Kitagawa, S. Kawata, *Inorg. Chem.* **2004**, *43*, 92.

[13] a) D. Braga, L. Brammerb, N. R. Champness, *CrystEngComm* **2005**, *7*, 1; b) C. B. Aakeröy, A. M. Beatty, B. A. Helfrich, *Angew. Chem.* **2001**, *113*, 3340; *Angew. Chem. Int. Ed.* **2001**, *40*, 3240; c) C. B. Aakeröy, *Acta Crystallogr. Sect. B* **1997**, *53*, 569; d) A. Angeloni, P. C. Crawford, A. G. Orpen, T. J. Podesta, B. J. Shore, *Chem. Eur. J.* **2004**, *10*, 3783; e) V. R. Vangala, B. R. Bhogala, A. Dey, G. R. Desiraju, C. K. Broder, P. S. Smith, R. Mondai, J. A. K. Howard, C. C. Wilson, *J. Am. Chem. Soc.* **2003**, *125*, 14495; f) S. G. Telfer, T. Sato, R. Kuroda, *Angew. Chem.* **2004**, *116*, 591; *Angew. Chem. Int. Ed.* **2004**, *43*, 581; g) S. G. Telfer, R. Kuroda, *Chem. Eur. J.* **2005**, *11*, 57.

[14] a) K. Adachi, S. Kaizaki, K. Yamada, S. Kitagawa, S. Kawata, *Chem. Lett.* **2004**, *33*, 648; b) S. Kawata, K. Adachi, Y. Sugiyama, M. K. Kabir, S. Kaizaki, *CrystEngComm* **2002**, *4*, 496; c) K. Adachi, Y. Sugiyama, H. Kumagai, K. Inoue, S. Kitagawa, S. Kawata, *Mol. Cryst. Liq. Cryst.* **2002**, *376*, 71; d) K. Adachi, Y. Sugiyama, H. Kumagai, K. Inoue, S. Kitagawa, S. Kawata, *Polyhedron* **2001**, *20*, 1411; e) K. Adachi, S. Kawata, M. K. Kabir, H. Kumagai, K. Inoue, S. Kitagawa, *Chem. Lett.* **2000**, 50.

[15] a) Y. Sugiyama, K. Adachi, M. K. Kabir, S. Kitagawa, T. Suzuki, S. Kaizaki, S. Kawata, *Mol. Cryst. Liq. Cryst.* **2002**, *379*, 419; b) Y. Sugiyama, K. Adachi, S. Kawata, H. Kumagai, K. Inoue, M. Katada, S. Kitagawa, *CrystEngComm* **2000**, *2*, 174.

[16] a) J. C. MacDonald, G. M. Whitesides, *Chem. Rev.* **1994**, *94*, 2383; b) G. M. Whitesides, *Sci. Am.* **1995**, 114; c) G. M. Whitesides, E. E. Simanek, J. P. Mathias, C. T. Seto, D. N. Chin, M. Mammen, D. M. Gordon, *Acc. Chem. Res.* **1995**, *28*, 37; d) A. Ranganathan, V. R. Pedireddi, C. N. R. Rao, *J. Am. Chem. Soc.* **1999**, *121*, 1752.

[17] a) A. D. Burrows, C.-W. Chan, M. M. Chowdhry, J. E. McGrady, D. M. P. Mingos, *Chem. Soc. Rev.* **1995**, *24*, 329; b) D. C. Sherrington, K. A. Taskinen, *Chem. Soc. Rev.* **2001**, *30*, 83.
[18] M. I. Tsushima, N. Nozaki, K. Ohno, *J. Phys. Chem. A* **2000**, *104*, 5176.
[19] G. M. Sheldrick, SHELXL97, University of Göttingen, Germany, **1997**.
[20] Gaussian 98, revision A.11.3, M. J. T. Frisch, G. W. Schlegel, H. B. Scuseria, G. E. Robb, M. A. Cheeseman, J. R. Zakrzewski, V. G. Montgomery, J. A. Stratmann, R. E. Burant, J. C. Dapprich, S. Millam, J. M. Daniels, A. D. Kudin, K. N. Strain, M. C. Farkas, O. Tomasi, J. Barone, V. Cossi, M. Cammi, R. Mennucci, B. Pomelli, C. Adamo, C. Clifford, S. Ochterski, J. Petersson, G. A. Ayala, P. Y. Cui, Q. Morokuma, K. Malick, D. K. Rabuck, A. D. Raghavachari, K. Foresman, J. B. Cioslowski, J. Ortiz, J. V. Stefanov, B. B. Liu, G. Liashenko, A. Piskorz, P. Komaromi, I. Gomperts, R. Martin, R. L. Fox, D. J. Keith, T. Al-Laham, M. A. Peng, C. Y. Nanayakkara, A. Gonzalez, C. Challacombe, M. Gill, P. M. W. Johnson, B. G. Chen, W. Wong, M. W. Andres, J. L. Head-Gordon, M. Replogle, J. A. Pople, Gaussian Inc, Pittsburgh, PA, **1998**.
[21] a) P. L. Flukiger, H. P. Portmann, S. Weber, J. Manno, MOLEKEL, Swiss Center for Scientific Computing, Switzerland, **2000**–**2002**; b) H. P. Portmann, *CHIMIA* **2000**, *54*, 755.
[22] S. Kawata, H. Kumagai, K. Adachi, S. Kitagawa, *J. Chem. Soc. Dalton Trans.* **2000**, 2409.
[23] The positive-mode ESI-MS spectrum of a THF solution of **4** in the presence of CsCl as a charge carrier shows formation of the triply hydrogen bonded module in THF solution, which is indicative of robustness of the building block (see Figure S-1 in the Supporting Information).
[24] a) S. Ikeuchi, K. Saito, Y. Nakazawa, A. Sato, M. Mitsumi, K. Toriumi, M. Sorai, *Phys. Rev. B* **2002**, *66*, 115110; b) K. Saito, Y. Yamamura, *Therm. Acta* **2005**, in press.
[25] H. B. Klevens, J. R. Platt, *J. Chem. Phys.* **1949**, *17*, 470.
[26] T. M. Azumi, *J. Chem. Phys.* **1962**, *37*, 2413.

Received: April 14, 2005
Published online: August 30, 2005

